Linear and nonlinear operation of a time-to-space processor

Dan M. Marom,* Dmitriy Panasenko, Pang-Chen Sun, and Yeshaiahu Fainman

Department of Electrical and Computer Engineering, University of California, San Diego, 9500 Gilman Drive, La Jolla, California 92093-0407

Received December 13, 1999; revised manuscript received July 5, 2000; accepted September 1, 2000

The operational characteristics of a time-to-space processor based on three-wave mixing for instantaneous imaging of ultrafast waveforms are investigated. We assess the effects of various system parameters on the processor's important attributes: time window of operation and signal conversion efficiency. Both linear and nonlinear operation regimes are considered, with use of a Gaussian pulse profile and a Gaussian spatial mode model. This model enables us to define a resolution measure for the processor, which is found to be an important characteristic. When the processor is operated in the linear interaction regime, we find that the conversion efficiency of a temporal signal to a spatial image is inversely proportional to the resolution measure. In the nonlinear interaction regime, nonuniform signal conversion due to fundamental wave depletion gives rise to a phenomenon that can be used to enhanced the imaging operation. We experimentally verify this nonlinear operation. © 2001 Optical Society of America

OCIS codes: 320.7100, 070.4340, 320.7110, 190.4380, 190.4420, 190.1900.

1. INTRODUCTION

Ultrafast temporal signals are difficult to acquire, as direct detection of the temporal information is impossible owing to the limited response time of existing solid-state optoelectronic photodetectors. Spatial imaging of ultrafast waveforms offers an invaluable ability, because the complex-amplitude temporal information is converted to a spatial distribution for subsequent detection by slower, parallel optoelectronic devices. Information about the temporal waveform envelope can be inferred from the detected one-dimensional spatial image. Recently, a single-shot technique for time-to-space conversion based on wave mixing spectrally decomposed waves (SDW's) has been introduced and experimentally demonstrated.[1] The time-to-space conversion is generated by three-wave mixing with the SDW of an information-carrying ultrashort temporal waveform and an inverted SDW of a reference ultrashort pulse in the Fourier plane of a spectral processing device (SPD) (see Fig. 1). The two SDW's in the Fourier plane are mixed in a $\chi^{(2)}$ crystal, generating a quasi-monochromatic wave at a doubled frequency. A spatial Fourier transform of the generated second-harmonic field to the output plane produces a spatial image, thereby performing a linear mapping of the information from the time-to-space domain. The novelty of this technique is that the usual relationship between the time window of observation and the physical aperture of the nonlinear crystal[2,3] is decoupled by spectral processing. Additionally, the spatially dispersed frequency components automatically compensate for group velocity mismatch, permitting high conversion efficiency.[4] Moreover quadratic phase compensation is achieved by displacing the output observation plane, permitting chirp cancellation in optical fiber transmissions.[5] These desirable features make this time-to-space converter suited for future ultrafast optical communication systems.[6]

In this paper, we study in detail the operation tradeoffs of the time-to-space converter. More specifically, we investigate the relationship between the conversion efficiency and the observation time window. This information is important in the design of an optical time-division multiplexing system based on ultrafast pulse packets. We find that the processor can be set to operate in the linear regime, under weak three-wave interaction, or in the nonlinear regime, where fundamental wave depletion is exhibited. For the linear regime we derive expressions for the output spatial signal and for the conversion efficiency, finding that the efficiency-resolution product of the processor is an invariant property; improving one parameter degrades the other. When the reference pulse power exceeds certain power levels, the spatial frequency bandwidth of the second harmonic broadens owing to nonuniform signal conversion. The nonlinear operation generates a spatial image with a narrower spot size than in the linear regime, resulting in an enhanced resolution output image due to the nonlinear signal processing.[7] We perform numerical simulations for this nonlinear conversion case based on a Gaussian pulse model and find the required reference pulse power levels for best temporal resolution and maximal conversion efficiency.

The paper is organized as follows: In Section 2 we establish the Gaussian beam profile and Gaussian pulse envelope model that is used throughout this paper, where we find the relationship between the size of the beam and the pulse duration to the resolution of the SPD. The linear and the nonlinear operating regimes of the time-to-space conversion processor are investigated in Sections 3

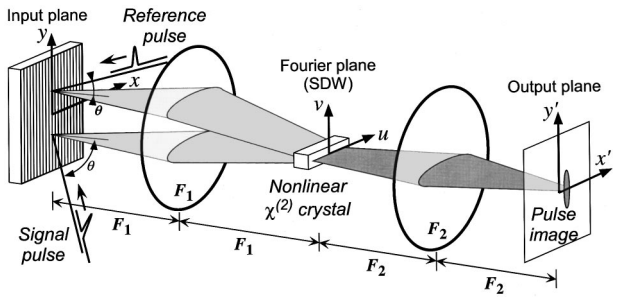

Fig. 1. Time-to-space conversion by using wave mixing of inverted spectrally decomposed waves from a signal and a reference pulse: F_1, F_2, focal length.

and 4, respectively. Experimental results verifying our analysis in terms of enhanced-resolution imaging are presented in Section 5, followed by a conclusion in Section 6.

2. GAUSSIAN MODEL OF INPUT WAVES

The signal and reference pulses that are used in the time-to-space conversion are introduced to the SPD from two opposite sides (see Fig. 1), such that the directions of their spatial dispersions will be mutually inverted. The beams carrying the signal and reference pulses are incident on the input grating of the SPD at angles of $+\theta$ and $-\theta$ relative to the input grating normal, respectively. The angle θ depends on the grating frequency and is chosen such that the diffracted wave at the center frequency of the ultrashort pulse is propagating along the optical axis of the SPD. The diffracted field immediately behind the grating for the signal pulse can be expressed as

$$U_{\text{in}}(x, y; t) = E_s w\left(\frac{x}{L_x}\right) w\left(\frac{y}{L_y}\right) p\left(\frac{t - t_0 - \alpha x/c}{\tau}\right) \times \exp(j\omega_0 t), \quad (1)$$

where $p(t)$ is the normalized temporal envelope of the ultrashort pulse and $w(x)$ and $w(y)$ are the normalized transversal beam profiles in the x and y directions (assuming that a separable function characteristic is applicable), defining the input pupil function. The parameters τ, L_x, and L_y characterize the pulse duration and the size of the input pupil function on the grating in the x and the y directions, respectively. In general, $L_x = L_y/\cos(\theta)$ if the input beam is circular, owing to the projection on the grating at angle θ. However, the beam can be anamorphically imaged on the grating to achieve independent control over L_x and L_y. The constants E_s, α, c, t_0, and ω_0 are the field strength, grating angular dispersion parameter [$\alpha = \sin(\theta)$], speed of light in vacuum, arbitrary time shift, and center angular frequency of the ultrashort pulse, respectively. Equation (1) describes a short pulse scanning across the fixed aperture at a velocity of c/α in the x direction. This velocity is greater than the speed of light in vacuum owing to the projection of the pulse front on a tilted plane.

We invoke the following two customary assumptions[8,9] in our study: temporal Gaussian pulse envelope and spatial Gaussian beam profile. The Gaussian beam profile is commonly used for spatial confinement of propagating waves and is a known solution to the paraxial Helmholtz equation.[10] The Gaussian pulse envelope is also found to be a good descriptor of ultrashort pulses. We define the pulse envelope and its corresponding temporal Fourier transform (TFT) by

$$p(t) = \exp\left(-\frac{t^2}{2}\right) \overset{\text{TFT}}{\Leftrightarrow} P(\omega) = \sqrt{2\pi}\exp\left(-\frac{\omega^2}{2}\right), \quad (2)$$

where ω is the angular frequency. Similarly, we define the Gaussian spatial beam profile and its corresponding spatial Fourier transform (SFT) by

$$w(x) = \exp(-x^2) \overset{\text{SFT}}{\Leftrightarrow} W(f_x) = \sqrt{\pi}\exp(-\pi^2 f_x{}^2), \quad (3)$$

where f_x is the spatial frequency. The difference between the TFT and SFT is due to the inclusion of 2π in the angular frequency term of the TFT, consistent with standard notation. Using the Gaussian model for the spatial modes and temporal profile, we rewrite Eq. (1) as

$$U_{\text{in}}(x, y; t) = E_s \exp\left(-\frac{x^2}{L_x{}^2}\right)\exp\left(-\frac{y^2}{L_y{}^2}\right) \times \exp\left[-\frac{1}{2\tau^2}\left(t - t_0 - \frac{\alpha x}{c}\right)^2\right]\exp(j\omega_0 t). \quad (4)$$

Let us make the following observation (see Fig. 2): The width of the spatial beam profile in the x direction is proportional to L_x. The instantaneous spatial width of the pulse scanning across the grating is proportional to $\sqrt{2}\tau c/\alpha$. The ratio of these two widths, $N \equiv \alpha L_x/\sqrt{2}\tau c$, is a measure of the resolution of the SPD and describes the number of pulses that fit into the input pupil function. Its significance is similar to the space–bandwidth product in a traditional spatial-domain optical processing system as will be illustrated next. (Note that N is identical to Weiner's resolution measure,[9] expressed using the parameters of our model.)

The input field of Eq. (4) undergoes a SFT by the first lens of the SPD, with focal length F_1, generating the field in the Fourier plane. The expression is simplified by using the resolution parameter N, yielding the temporal field in local spatial coordinates u and v:

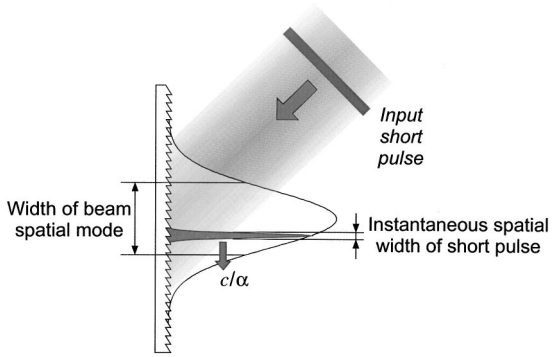

Fig. 2. Gaussian beam mode and Gaussian pulse envelope incident on the diffraction grating. The ratio of their spatial widths determines the resolution of the system.

$$U_{\mathrm{SDW}}(u,\nu;t) = \frac{E_s L_x L_y \pi}{\lambda_0 F_1 \sqrt{1+N^2}} \exp\left[-\frac{(t-t_0)^2}{2\tau^2(1+N^2)}\right] \times \exp\left[-\left(\frac{L_x \omega_0 u}{2cF_1}\right)^2 \frac{1}{1+N^2}\right] \times \exp\left[-\left(\frac{L_y \omega_0 \nu}{2cF_1}\right)^2\right] \times \exp\left[-j\frac{2\pi}{\lambda_0}\frac{cu}{\alpha F_1}\frac{N^2}{1+N^2}(t-t_0)\right] \times \exp(j\omega_0 t). \quad (5)$$

A TFT can be applied to Eq. (5), revealing the spatial dispersion of the field, given by

$$\tilde{U}_{\mathrm{SDW}}(u,\nu,\omega) = \frac{E_s L_x L_y \pi \tau \sqrt{2\pi}}{\lambda_0 F_1} \exp\left[-\frac{\tau^2}{2}(1+N^2) \times \left(\omega - \omega_0 + \frac{u\omega_0}{\alpha F_1}\frac{N^2}{1+N^2}\right)^2\right] \times \exp\left[-\left(\frac{L\omega_0 u}{2cF_1}\right)^2 \frac{1}{1+N^2}\right] \times \exp\left[-\left(\frac{L\omega_0 \nu}{2cF_1}\right)^2\right] \exp[-j(\omega-\omega_0)t_0]. \quad (6)$$

Note that optical fields in the temporal frequency domain are denoted with a tilde overscript, $\tilde{U}$. Equations (5) and (6) are the time domain and frequency domain representations of the spectrally decomposed wave[11] (SDW) at the Fourier plane. Some important observations can be made on the properties of the SDW from inspecting Eqs. (5) and (6): (i) From Eq. (5) we learn that the duration of the SDW is increased by a factor of $\sqrt{1+N^2}$. This time corresponds to the time of flight of the pulse through the aperture in the input plane (see Fig. 2). (ii) The spatial dispersion of the temporal frequency components are observed in the first Gaussian function of Eq. (6), yielding $\mathrm{d}\omega/\mathrm{d}u = -(\omega_0/\alpha F_1)N^2/(1+N^2)$. The spatial dispersion is manifest in Eq. (5) as a Doppler shift of the temporal frequency as a function of the spatial coordinate u. The Doppler frequency shift arises from the movement of the input pulse (or light source) across the diffraction grating. This movement also leads to (iii) The phase fronts of the SDW field [Eq. (5)] vary as a function of time, and the instantaneous angle between the wave vector and the optical axis of the SPD in the paraxial approximation is $(c/\alpha F_1)(N^2/1+N^2)(t-t_0)$. (iv) The temporal bandwidth at any location u is determined by the first Gaussian function of Eq. (6) and is a $(1+N^2)^{1/2}$ fraction of the total bandwidth. The frequency resolution can be calculated by dividing the total width of the field [given by the second Gaussian function of Eq. (6)] by the width for a single temporal-frequency component (given by the first Gaussian function when substituting $\omega = \omega_0$, for example). This ratio is again found to be $(1+N^2)^{1/2}$. In the limit of high-resolution operation (i.e., $N \gg 1$), we will observe that the SDW duration is $N\tau$, the bandwidth at any point has decreased by a factor of N, and the spatial resolution of frequency components is N. In contrast, if we operate at the low-resolution limit (i.e., $N \ll 1$), the SDW duration will be the same as that of the incident pulse (i.e., τ), and there will be no spatially varying Doppler shift term and no spatial resolution of the frequency components. In this low-resolution case, monochromatic diffraction effects are more pronounced than the bandwidth of the optical source.[10]

As a last step, we calculate the confocal length of the SDW, required as an approximate limit to the possible interaction length in the wave-mixing process under Gaussian beam focusing. The confocal length is calculated from the spatial width (or waist) of the SDW [from Eq. (5)]. The field distribution obeys an independent Gaussian mode for the u and ν directions or an elliptical cross section. We find that the two independent confocal lengths for the u and the ν directions are $2Z_{0u} = 2n_{\omega_0}{F_1}^2\lambda_0(1+N^2)/\pi{L_x}^2$ and $2Z_{0\nu} = 2n_{\omega_0}{F_1}^2\lambda_0/\pi{L_y}^2$, respectively, where n_{ω_0} is the refractive index of the crystal at frequency ω_0. If one of the confocal lengths is significantly smaller than the other, then it serves as the limit to the interaction length. Usually $L_x \approx L_y$ and $N \gg 1$, resulting in $2Z_{0\nu}$ as the limiting interaction length. As the size of the input pupil is increased, the confocal length is decreased.

The characteristics of the spectrally decomposed waves are required in our analysis of the time-to-space conversion, which is evaluated in Sections 3 and 4 in the linear and the nonlinear regimes.

3. LINEAR TIME-TO-SPACE CONVERSION

In this section we analyze the wave-mixing process and the dependence of the spatial output signal on the parameters of the SPD in the linear regime, where the fundamental input waves are nondepleting. When this assumption is used, the SDW of the signal and reference pulses are completely characterized and we may find the nonlinear polarization term that arises in the nonlinear crystal. Armed with the nonlinear polarization, we solve the wave equation for the generated quasi-monochromatic third wave, whose spatial frequency modulation carries the temporal-frequency information of the signal pulse. This resultant wave undergoes a SFT to the output plane of the SPD, giving rise to a spatial signal that contains the desired temporal location information t_0 (see Fig. 1). Finally, we calculate the total energy that has been converted to the spatial domain, from which we can find the conversion efficiency from the input temporal pulse to the output spatial signal. This approach differs from Weiner's conversion efficiency estimation, which is based on the SDW's averaged power density[4] (averaged in duration and distribution). We believe that our approach is justified since the conversion is produced by a fast parametric point process, and therefore one should take into account the temporal dynamics and field distribution of the SDW's, as evaluated in Section 2.

A. Nonlinear Polarization

The two mutually inverted SDW's of the signal pulse and the reference pulse interact by using a three-wave-mixing process in a crystal exhibiting a second-order nonlinearity. Since we are operating in the linear interaction regime, the analysis can be performed in the temporal frequency domain. Therefore the nonlinear polarization can be expressed as a convolution of the two input waves in the temporal frequency domain. The SDW of the signal pulse in the temporal frequency domain is given by Eq. (6). The reference pulse generates a similar SDW with an inverted spatial dispersion sign. Consequently, we can express the nonlinear polarization term as[12]

$$P^{\mathrm{NL}}(u,\nu,z;\omega) = 2\epsilon_0 d_{\mathrm{eff}} \int_{-\infty}^{\infty} \tilde{U}^{S}_{\mathrm{SDW}}(u,\nu;\varpi)\tilde{U}^{R}_{\mathrm{SDW}}(u,\nu;\omega-\varpi) \times \exp[j[k_S(\varpi)+k_R(\omega-\varpi)]z]\mathrm{d}\varpi, \quad (7)$$

where d_{eff} is the nonlinear optical coefficient, which is assumed to be constant across the interaction bandwidth as a nonresonant nonlinearity is used, S and R denote the signal and the reference SDW waves, $k_S(\cdot)$ and $k_R(\cdot)$ are the wave-vector magnitudes as a function of the temporal frequency, and the integration variable ϖ has units of temporal frequency. We express the wave-vector dependence on a temporal frequency variable Ω by using a Taylor series expansion about $\Omega = \omega_0$, yielding

$$k_S(\varpi) = k(\omega_0) + (\varpi-\omega_0)\left.\frac{\partial k(\Omega)}{\partial\Omega}\right|_{\Omega=\omega_0} + \ldots,$$

$$k_R(\omega-\varpi) = k(\omega_0) + (\omega-\varpi-\omega_0)\left.\frac{\partial k(\Omega)}{\partial\Omega}\right|_{\Omega=\omega_0} + \ldots.$$

(Note: we assume a type I interaction where the two fundamental waves are polarized parallel to the crystal's ordinary axis. Therefore the Taylor coefficients for the two expansions are identical.) When we express the sum of the two k vectors by using only the first two terms of the series expansion, the resultant can be shown to be independent of ϖ and can therefore be taken out of the integral. The nonlinear polarization can therefore be approximated by

$$P^{\mathrm{NL}}(u,\nu,z;\omega) = 2\epsilon_0 d_{\mathrm{eff}} \exp\left\{ j\left[2k(\omega_0) + k(\omega-2\omega_0)\left.\frac{\partial k(\Omega)}{\partial\Omega}\right|_{\Omega=\omega_0}\right] z\right\} G(u,\nu;\omega), \quad (8)$$

where

$$G(u,\nu;\omega) = \int_{-\infty}^{\infty} \tilde{U}^{S}_{\mathrm{SDW}}(u,\nu;\varpi)\tilde{U}^{R}_{\mathrm{SDW}}(u,\nu;\omega-\varpi)\mathrm{d}\varpi$$

is the convolution operation in the temporal frequency domain.

B. Generated Wave

The nonlinear polarization of Eq. (8) serves as the driving force for the wave equation of the generated third wave, governed by[12]

$$\frac{\partial}{\partial z}\tilde{U}_{\mathrm{sum}}(u,\nu,z;\omega) = \frac{j}{2}\frac{\omega^2\mu_0}{k(\omega)}P^{\mathrm{NL}}(u,\nu,z;\omega) \times \exp[-jk_{\mathrm{sum}}(\omega)z], \quad (9)$$

which is the differential equation obtained from the monochromatic plane-wave solution, when the slowly varying envelope and nondepleting pump approximations are used. We next expand $k_{\mathrm{sum}}(\omega)$ in a Taylor series about $\Omega = 2\omega_0$, keeping only the first two terms of the expansion. This procedure is carried out for the phase term only, because it will oscillate rapidly with propagation along z. Using the Taylor approximation and inserting the nonlinear polarization of Eq. (8) into Eq. (9) yields

$$\frac{\partial}{\partial z}\tilde{U}_{\mathrm{sum}}(u,\nu,z;\omega) = j\frac{2\omega_0}{cn_{2\omega_0}}d_{\mathrm{eff}}G(u,\nu;\omega) \times \exp[-j[k(2\omega_0)-2k(\omega_0)]z]\exp\{-j(\omega-2\omega_0) \times [(\partial k/\partial\Omega)|_{\Omega=2\omega_0}-(\partial k/\partial\Omega)|_{\Omega=\omega_0}]z\}. \quad (10)$$

We assume that the phase-matching condition, $k(2\omega_0) = 2k(\omega_0)$, can be satisfied by proper crystal selection and orientation. Equation (10) can be integrated from 0 to L_c, the length of the crystal, assuming a zero initial state [i.e., $\tilde{U}_{\mathrm{sum}}(u,\nu,0;\omega) = 0$]. The field outside the output face of the crystal is given by

$$\bar{U}_{\mathrm{sum}}(u,\nu,L_c;\omega) = j\frac{2\omega_0}{cn_{2\omega_0}}E_sE_r\sqrt{n_{2\omega_0}}\left(\frac{L_xL_y\pi\tau\sqrt{2\pi}}{\sqrt{n_{\omega_0}}\lambda_0F_1}\right)^2 \times \frac{\sqrt{\pi}}{\tau\sqrt{1+N^2}}d_{\mathrm{eff}}L_c\exp\left[-2\left(\frac{L_y\omega_0\nu}{2cF_1}\right)^2\right] \times \exp\left[-\frac{2}{1+N^2}\left(\frac{L_x\omega_0u}{2cF_1}\right)^2\right]\exp\left[-\frac{{t_0}^2}{4\tau^2(1+N^2)}\right] \times \exp\left[j\omega_0t_0\frac{u}{\alpha F_1}\frac{N^2}{1+N^2}\right]A(\omega) \quad (11)$$

with $A(\omega)$ defined by

$$A(\omega) = \exp\left[-\frac{(\omega-2\omega_0)^2\tau^2}{2}\frac{1+N^2}{2}\right] \times \mathrm{sinc}\left[(\omega-2\omega_0)\frac{\beta L_c}{2}\right] \times \exp\left[-j(\omega-2\omega_0)\frac{\beta L_c+t_0}{2}\right], \quad (12)$$

where $\beta = (\partial k/\partial\Omega)|_{\Omega=2\omega_0} - (\partial k/\partial\Omega)|_{\Omega=\omega_0}$ is the inverse group velocity mismatch and we used the explicit solution

of the convolution $G(u, \nu; \omega)$ in deriving Eq. (11). We observe that the spatial dependence of the output signal has been decoupled from the temporal-frequency variable. This is a fundamental property of wave mixing two mutually inverted SDW's. The spatial dependence in Eq. (11) contains the following components: (i) a confined spatial extent prescribed by the spatial Gaussian functions, (ii) an attenuation factor with Gaussian dependence on the time delay t_0 between the signal and the reference pulses, and (iii) a spatial linear phase term that carries the timing information t_0. The temporal-frequency dependence of $A(\omega)$ consists of the generated Gaussian bandwidth multiplied by a spectral filter in the form of the sinc function. The generated sum wave can also be expressed in the time domain when an inverse TFT is performed, which would result in the replacement of $A(\omega)$ in Eq. (11) by $a(t)$, given by

$$a(t) = \frac{\exp(j2\omega_0 t)}{\sqrt{\pi}\tau\beta L_c\sqrt{1+N^2}}\exp\left[-\frac{(t-t_0/2)^2}{\tau^2(1+N^2)}\right] \otimes \mathrm{rect}\left(\frac{t}{\beta L_c}-\frac{1}{2}\right). \tag{13}$$

Since the TFT of a product is a convolution, $a(t)$ is defined by a convolution between Gaussian and rectangular temporal envelopes with a center frequency of $2\omega_0$. In the case that $\beta L_c \ll \tau N$, spectral filtering due to group velocity mismatch will be negligible and the spectrum $A(\omega)$ and the temporal profile $a(t)$ will be Gaussian. In contrast, when $\beta L_c \gg \tau N$, the spectrum will have a sinc dependence due to phase-matching considerations and the temporal profile will be rectangular.

C. Output Spatial Signal

The field at the output plane of the SPD is evaluated by the SFT of the generated field from the three-wave-mixing process. We express this output field in the time domain, yielding

$$\begin{aligned} U_{\mathrm{out}}(x', y'; t) &= j\frac{d_{\mathrm{eff}}}{\sqrt{n_{2\omega_0}n_{\omega_0}}}2^3\pi^{7/2}E_sE_r\frac{L_xL_y\tau}{{\lambda_0}^2F_2}L_c a(t) \\ &\times \exp\left[-\frac{{t_0}^2}{4\tau^2(1+N^2)}\right]\exp\left[-2\left(\frac{F_1}{F_2}\frac{y'}{L_y}\right)^2\right] \\ &\times \exp\left[-2\left(\frac{F_1}{F_2}\right)^2\frac{1+N^2}{{L_x}^2}\left(x'-\frac{ct_0}{2\alpha}\frac{F_2}{F_1}\frac{N^2}{1+N^2}\right)^2\right]. \end{aligned} \tag{14}$$

The last two Gaussian terms in Eq. (14) characterize the spot size of the output spatial signal. The location of this Gaussian signal is determined by the temporal information t_0, weighted by the SPD parameters. This term represents the time-to-space converted signal. The amplitude of the output signal is weighted by the Gaussian time window of the SPD, limiting the possible values of t_0. The resolution of the time-to-space converter is determined by these two parameters. It can be shown that the ratio of the spatial widths of the observed range of output values to the spot size reduces exactly to N, the resolution of the SPD. This result is consistent with our linear conversion regime, illustrating that the space–bandwidth product is preserved. We next analyze the conversion efficiency of the processor.

D. Conversion Efficiency

The time-to-space processor functions in real time, generating the time-varying output spatial field. However, all detection devices respond to the optical intensity. The time-dependent intensity is calculated from Eq. (14), where the amplitudes of the signal and reference pulses have been expressed by their relationship to the signal and the reference pulse energies $\mathcal{E}_s$ and $\mathcal{E}_r$, respectively (see Appendix A) along with the definitions relating the refractive index, the electric permeability, and the speed of light in vacuum, yielding

$$\begin{aligned} I_{\mathrm{out}}(x', y'; t) &= \frac{1}{2}\sqrt{\frac{\epsilon_0}{\mu}}|U_{\mathrm{out}}(x', y'; t)|^2 \\ &= \frac{d_{\mathrm{eff}}^2}{n_{2\omega_0}n_{\omega_0}^2}\frac{1}{\epsilon_0 c}\frac{2^9\pi^4}{{\lambda_0}^4{F_2}^2}\mathcal{E}_s\mathcal{E}_r{L_c}^2|a(t)|^2 \\ &\times \exp\left[-\frac{{t_0}^2}{2\tau^2(1+N^2)}\right] \\ &\times \exp\left[-4\left(\frac{F_1}{F_2}\frac{y'}{L_y}\right)^2\right] \\ &\times \exp\left[-4\left(\frac{F_1}{F_2}\right)^2\frac{1+N^2}{L^2} \right. \\ &\left. \times \left(x'-\frac{ct_0}{2\alpha}\frac{F_2}{F_1}\frac{N^2}{1+N^2}\right)^2\right]. \end{aligned} \tag{15}$$

Using the expression for the intensity distribution, we find the total energy at the output, yielding

$$\begin{aligned} \mathcal{E}_{\mathrm{out}} &= \int_{-\infty}^{\infty}\int_{-\infty}^{\infty}\int_{-\infty}^{\infty} I_{\mathrm{out}}(x', y'; t)\mathrm{d}x\mathrm{d}y\mathrm{d}t \\ &= \frac{d_{\mathrm{eff}}^2}{n_{2\omega_0}n_{\omega_0}^2}2^7\pi^5\mathcal{E}_s\mathcal{E}_r\frac{1}{\epsilon_0 c}\frac{L_xL_y{L_c}^2}{{\lambda_0}^4{F_1}^2\sqrt{1+N^2}} \\ &\times \exp\left[-\frac{{t_0}^2}{2\tau^2(1+N^2)}\right]\int_{-\infty}^{\infty}|a(t)|^2\mathrm{d}t, \end{aligned} \tag{16}$$

which can be simplified with Parseval's relationship,

$$\begin{aligned} \int_{-\infty}^{\infty}|a(t)|^2\mathrm{d}t &= \frac{1}{2\pi}\int_{-\infty}^{\infty}|A(\omega)|^2\mathrm{d}\omega \\ &= \frac{1}{2\pi}\int_{-\infty}^{\infty}\exp\left[-\frac{\Omega^2\tau^2}{2}(1+N^2)\right] \\ &\times \mathrm{sinc}^2\left(\Omega\frac{\beta L_c}{2}\right)\mathrm{d}\Omega, \end{aligned} \tag{17}$$

with a change of integration variable $\Omega = \omega - 2\omega_0$. The output energy can be expressed in analytic form for

two limiting cases, when the spectral filtering is negligible ($\beta L_c \ll \tau N$) or dominant ($\beta L_c \gg \tau N$).

In the limit of a high-resolution SPD (i.e., a large pupil mode size, leading to $N \gg 1$), which is usually the case of interest, the Gaussian spectrum will be much narrower than the sinc function. We find that the output energy is given by

$$\mathcal{E}_{\text{out}} = \frac{d_{\text{eff}}^2}{n_{2\omega_0} n_{\omega_0}^2} 2^{13/2} \pi^{9/2} \mathcal{E}_s \mathcal{E}_r \frac{1}{\epsilon_0 c} \frac{{L_c}^2}{{\lambda_0}^4 {F_1}^2} \frac{L_x L_y}{\tau N^2} \times \exp\left(-\frac{{t_0}^2}{2\tau^2 N^2} \right). \quad (18)$$

The actual interaction length in the crystal L_c, is determined by the minimum of either one of the two confocal lengths of the SDW or the actual length of the crystal.

The output energy can also be evaluated for the case of a very small pupil mode size. In this case, spectral filtering due to the group velocity mismatch will be predominant in Eq. (17). This extreme case is of no interest to us because there is no time-to-space conversion.

E. Efficiency-Resolution Product

Let the conversion efficiency be defined as $\eta = \mathcal{E}_{\text{out}}/\mathcal{E}_s$, the total energy converted from the time-to-space domains. We can manipulate Eq. (18) to express the product of the conversion efficiency and N, the resolution of the SPD. After simplifying we find that

$$\eta N = \frac{d_{\text{eff}}^2}{n_{2\omega_0} \eta_{\omega_0}^2} 2^7 \pi^{9/2} \mathcal{E}_r \frac{{L_c}^2}{{\lambda_0}^4 {F_1}^2} \frac{L_y}{\epsilon_0 \alpha} \exp\left(-\frac{{t_0}^2}{2\tau^2 N^2} \right). \quad (19)$$

Thus the efficiency-resolution product is invariant to L_x. One parameter can be improved at the expense of the other, under the assumption that L_c is less than the confocal distance. The implication of this result is that the performance can be improved by increasing L_y and/or decreasing F_1, resulting in tighter focusing of the SDW. However, this leads to a reduction in the confocal length.

In the limiting case of confocal focusing, where we choose the interaction length to equal the confocal length in the vertical direction as defined in Section 2 (because it is shorter than the confocal length in the horizontal direction when $L_x \approx L_y$), we find that

$$\eta N = \frac{d_{\text{eff}}^2}{n_{2\omega_0}} 2^9 \pi^{5/2} \frac{\mathcal{E}_r}{\epsilon_0} \frac{{F_1}^2}{\alpha {L_y}^3 {\lambda_0}^2} \exp\left(-\frac{{t_0}^2}{2\tau^2 N^2} \right). \quad (20)$$

It is possible to define $f\# = F_1/L_y$, and conclude that the performance of the time-to-space converter improves as $f\#$ increases. Since $L_y \approx L_x$ and $N \propto L_x$, for a large time window to be converted to a space-domain image with a confocal crystal length, a severe conversion efficiency penalty must be paid.

The invariance of the efficiency-resolution product to L_x could be intuitively explained by the following reasoning: The duration of the input field to the SPD is proportional to L_x (input spatial mode), while the field amplitude is proportional to $1/\sqrt{L_x}$ (see Appendix A). The corresponding SDW has the same dependence on L_x for both amplitude and duration parameters. The amplitude of the generated second-harmonic field under the linear conversion regime is therefore proportional to $1/L_x$, while the duration is still proportional to L_x. The power of the generated field is proportional to $1/{L_x}^2$ with no change in the duration. Consequently, the energy of the spatial signal is proportional to $1/L_x$, as is the conversion efficiency. Since the resolution N is proportional to L_x, the efficiency-resolution product is invariant to L_x.

The expressions derived in this subsection are valid for weak interaction leading to the linear conversion behavior. However, in many practical cases of interest, the analyzed ultrafast signal is much weaker than the reference pulse. While this arrangement can lead to a high conversion efficiency, it may violate our basic assumption of linear interaction with nondepleting fundamental waves. Therefore a complete analysis should allow fundamental wave depletion, and it is conducted in Section 4.

4. NONLINEAR TIME-TO-SPACE CONVERSION

The three-wave-mixing process of the time-to-space converter is reexamined in this section under the assumption of a strong reference pulse interacting with a weak signal pulse. The reference pulse's SDW is considered to be nondepleting, while the SDW of the signal pulse and the generated quasi-monochromatic second-harmonic wave will experience periodic power exchanges. Owing to the temporal dynamics of the interacting waves, the analysis needs to be performed in the time domain (as opposed to the temporal frequency domain of Section 3), requiring the introduction of a time derivative to the coupled-wave equations. We resolve this complication by restricting our solution to the high-resolution case, where the temporal bandwidth of the waves at any spatial location decreases and approaches a quasi-monochromatic wave. Thus we can use the quasi-static solution to solve the wave-mixing process, ignoring the effect of group velocity mismatch (more thorough justification provided in Appendix B).

A. High-Resolution Spectrally Decomposed Waves

A general expression for the signal pulse's SDW in the high-resolution limit can be evaluated by the SFT of Eq. (1), yielding

$$U_{\text{SDW}}^S(u, \nu; t) = \frac{E_s L_y c\tau}{\alpha \lambda_0 F_1} W\left(\frac{\omega_0 L_y \nu}{2\pi c F_1} \right) w\left[\frac{c(t - t_0)}{\alpha L_x} \right] \times P\left(-\frac{u\tau\omega_0}{\alpha F_1} \right) \exp\left[-j \frac{\omega_0 u}{\alpha F} (t - t_0) \right] \exp(j\omega_0 t), \quad (21)$$

where $W(\cdot)$ and $P(\cdot)$ are the SFT and the TFT of $w(\cdot)$ and $p(\cdot)$, respectively. In our limiting case of high-resolution SDW, the spatial extent in the x direction of the moving ultrashort pulse in Eq. (1) is much smaller than the size of the beam. Thus, in deriving Eq. (21), we simplified the Fourier integral by sampling the spatial mode at the location of the short pulse and taking the aperture effect out of the integral. The temporal frequency dependence of the SDW, evaluated by the TFT of Eq. (21), is given by

$$U^{S}_{\mathrm{SDW}}(u,\nu;\omega) = \frac{E_s L_x L_y \tau}{\lambda_0 F_1} W\left(\frac{\omega_0 L_y \nu}{2\pi c F}\right) W\left[\frac{\alpha L_x \omega_0}{c}\left(\frac{\omega}{\omega_0} - 1 + \frac{u}{\alpha F_1}\right)\right] \times P\left(-\frac{u\tau\omega_0}{\alpha F_1}\right)\exp[-j(\omega-\omega_0)t_0]. \quad (22)$$

The term mixing the temporal frequency components with the spatial coordinate u in the SFT of the input aperture characterizes the spatial dispersion. Since the beam aperture L_x is large in the high-resolution case, its SFT is a very narrow function. Its width determines the temporal frequency overlap or bandwidth $\Delta\omega$ at any point on the spatial coordinate u. The center temporal frequency component at the spatial coordinate u for the signal SDW is given by

$$\omega_{\mathrm{sig}} = \omega_0 - \frac{u\omega_0}{\alpha F}. \quad (23a)$$

The reference pulse SDW can be described by expressions similar to Eqs. (21) and (22), yet with an opposite spatial dispersion direction. Its temporal frequency to spatial coordinate relationship is therefore given by

$$\omega_{\mathrm{ref}} = \omega_0 + \frac{u\omega_0}{\alpha F}. \quad (23b)$$

We next calculate the phase mismatch of the wave-mixing process at an arbitrary spatial location u due to the temporal frequency bandwidth.

B. Phase Mismatch in Wave-Mixing High-Resolution Spectrally Decomposed Waves

The phase mismatch between the generated spatial wave and the two fundamental SDW's at any spatial location is a function of the wave-vector dependence on temporal frequency. We express this dependence by a Taylor expansion about ω_0 for the fundamental SDW and about $2\omega_0$ for the generated second-harmonic wave, as has been done in the linear analysis case. When the Taylor expansions are used, the phase mismatch is given by

$$\begin{aligned}\Delta k &= k_{\mathrm{sum}}(\omega_{\mathrm{sig}} + \delta\omega_s + \omega_{\mathrm{ref}} + \delta\omega_r) - k_S(\omega_{\mathrm{sig}} + \delta\omega_s) - k_R(\omega_{\mathrm{ref}} + \delta\omega_r)\\ &= \left[k(2\omega_0) + \left.\frac{\mathrm{d}k}{\mathrm{d}\omega}\right|_{2\omega_0}(\omega_{\mathrm{sig}} + \omega_{\mathrm{ref}} - 2\omega_0 + \delta\omega_s + \delta\omega_r)\right] - \left[k(\omega_0) + \left.\frac{\mathrm{d}k}{\mathrm{d}\omega}\right|_{\omega_0}(\omega_{\mathrm{sig}} - \omega_0 + \delta\omega_s)\right]\\ &\quad - \left[k(\omega_0) + \left.\frac{\mathrm{d}k}{\mathrm{d}\omega}\right|_{\omega_0}(\omega_{\mathrm{ref}} - \omega_0 + \delta\omega_r)\right]\\ &= [k(2\omega_0) - 2k(\omega_0)] + \beta\cdot(\omega_{\mathrm{sig}} + \omega_{\mathrm{ref}} - 2\omega_0 + \delta\omega_s + \delta\omega_r)\\ &= \beta\cdot(\delta\omega_s + \delta\omega_r) \leqslant \beta\cdot|\Delta\omega|, \end{aligned} \quad (24)$$

where $\delta\omega_s$ and $\delta\omega_r$ are frequency terms that are contained in the bandwidth $\Delta\omega$ at each spatial location for the signal and reference SDW. Equation (24) states that the phase mismatch is bound by the product of the inverse group velocity mismatch β (defined in Subsection 3.B) and the bandwidth $\Delta\omega$ at any point on the spatial coordinate u. Since the bandwidth is inversely proportional to L_x, the phase mismatch can be reduced by increasing L_x until the effect of this phase mismatch can be ignored (see Appendix B). In deriving the phase mismatch bound of Eq. (24), we assume that the constant term of the phase mismatch is eliminated by proper crystal orientation, set to satisfy the phase-matching condition. Additionally, owing to the opposite spatial dispersion directions, $\omega_{\mathrm{sig}} + \omega_{\mathrm{ref}} = 2\omega_0$ [see Eqs. (23a) and (23b)]. Finally, $\delta\omega_s$ and $\delta\omega_r$ are bound on $(-\Delta\omega/2, \Delta\omega/2)$ such that their sum is always less than or equal to $|\Delta\omega|$.

C. Solution of Nonlinear Wave-Mixing Spectrally Decomposed Waves

By increasing the SDW resolution, both the bandwidth and phase mismatch at each location are reduced, such that we can assume that in the high-resolution limit the waves are essentially quasi-monochromatic and the three interacting waves are phase matched. Thus the nonlinear wave-mixing problem can be treated with the quasi-static approximation, with the differential equations characterizing the three wave mixing defined by[12]

$$\begin{aligned}\frac{\partial}{\partial z}U^{S}_{\mathrm{SDW}}(u,\nu,z;t) &= j\frac{\omega_0}{cn_{\omega_0}}d_{\mathrm{eff}}U_{\mathrm{sum}}(u,\nu,z;t)U^{R*}_{\mathrm{SDW}}(u,\nu;t),\\ \frac{\partial}{\partial z}U_{\mathrm{sum}}(u,\nu,z;t) &= j\frac{2\omega_0}{cn_{2\omega_0}}d_{\mathrm{eff}}U^{S}_{\mathrm{SDW}}(u,\nu,z;t)U^{R}_{\mathrm{SDW}}(u,\nu;t), \end{aligned} \quad (25)$$

where we assume that the SDW arising from the reference pulse $U^{R}_{\mathrm{SDW}}(u,\nu;t)$ is nondepleting. This set of coupled equations resemble those of the frequency-sum process with monochromatic plane waves, and their solution is known to be oscillatory with respect to z. We apply the oscillatory solution with zero initial condition for the generated sum wave, yielding

$$U_{\mathrm{sum}}(u,\nu,z;t) = j\sqrt{\frac{2n_{\omega_0}}{n_{2\omega_0}}}\frac{U^{R}_{\mathrm{SDW}}(u,\nu;t)}{|U^{R}_{\mathrm{SDW}}(u,\nu;t)|}U^{S}_{\mathrm{SDW}}(u,\nu,z=0;t) \times \sin\left(\sqrt{\frac{2\omega_0^2}{c^2 n_{\omega_0} n_{2\omega_0}}}d_{\mathrm{eff}}|U^{R}_{\mathrm{SDW}}(u,\nu;t)|z\right). \quad (26)$$

One can make a small-signal approximation (i.e., $\sin(x) = x$], yielding the results for the linear time-to-space conversion process in the case of negligible spectral filtering (or high resolution). A general form of the SDW, see Eq. (21), or a Gaussian pulse and Gaussian spatial mode

model, see Eq. (5) with $N \gg 1$, can be used in Eq. (26) to characterize the generated wave. However, the nonlinear relationship on the amplitude of the reference SDW prohibits continuing the analysis to the output plane of the processor. Moreover, the reference SDW amplitude is time varying according to the spatial mode of the input beam. A computation program can calculate the SFT of the field at the output of a crystal of length L_c at all times t to generate the field at the observation plane. With the time-varying field, the detected instantaneous intensity can be computed as well as the total energy conversion from the input signal pulse energy to the output spatial wave energy.

However, we can calculate the conversion efficiency from Eq. (26). Using the relationship relating field and intensity, we find that

$$I_{\mathrm{sum}}(u, \nu, L_c; t) = 2I^{S}_{\mathrm{SDW}}(u, \nu, 0; t)\sin^2\left\{2\pi \frac{d_{\mathrm{eff}} L_c}{\lambda_0}\left[\frac{4I^{R}_{\mathrm{SDW}}(u, \nu; t)}{\epsilon_0 c n_{2\omega_0} n_{\omega_0}{}^2}\right]^{1/2}\right\} \tag{27}$$

For total conversion efficiency, Eq. (27) needs to be integrated over the spatial and the temporal extent. The factor of 2 arises from an equal energy contribution from the reference SDW for every converted photon from the signal SDW.

D. Modeling and Numerical Solution

To characterize the nonlinear time-to-space conversion, a program for calculating the output spatial signal and its accompanying properties was employed, by using a Gaussian pulse envelope and a rectangular beam profile. The rectangular window eliminates the temporal variations of the reference pulse amplitude, simplifying the calculations. Since we are interested in qualitative insight into the nonlinear conversion effect, we computed the output spatial signal from a generated signal of the form $\exp(-x^2)\sin[K\exp(-x^2)]$. The parameter K accounts for the amplitude of u_{ref}, the nonlinear optical coefficient d_{eff}, and the other constants such as the crystal length and refractive indices in Eq. (26). The magnitude squared of the Fourier transform of the output field represents the output intensity distribution observed in the time-to-space conversion.

The results of the simulation (see Fig. 3) illustrate the following: For small values of K the sine function behaves linearly and the generated wave is weak. Its shape is of a smooth Gaussian envelope, both in the Fourier transform plane and at the output plane. As the value of K increases, the generated wave in the Fourier plane exhibits a nonlinear amplitude increase across its spatial distribution. The increase rate is reduced near the center of the Gaussian mode and approaches its maximal value, in accordance with a sine function behavior. Consequently, owing to the Fourier transform relationship, the corresponding pulse image at the output becomes narrower. This image-narrowing feature signifies an improvement in the resolution capability of the time-to-space converter, as the total time window did not change. For greater values of K a dip in the generated wave is developed due to a downconversion process of photons that have been initially generated in a frequency-sum process. For large values of K, complete modulation of the Gaussian spatial mode occurs, resulting in two separate Gaussian diffraction spots. The phenomenon of a nonuniform signal depletion across the transverse spatial profile is also observed when focusing beams for second-harmonic generation and optical parametric amplification experiments.[13–15] Figure 4 shows a comparison of the output image's spatial distribution by superimposing the normalized traces for small K (linear conversion) and $K = 2.5$ (nonlinear conversion). The image-narrowing feature, resulting in enhanced resolution, is clearly evident.

Two criteria were used to compare the output images: A FWHM measure and a normalized second moment of the profile, i.e.,

$$\int_{-\infty}^{\infty} x^2 I_{\mathrm{out}}(x)\,\mathrm{d}x \Big/ \int_{-\infty}^{\infty} I_{\mathrm{out}}(x)\,\mathrm{d}x.$$

A plot of the two width criteria as a function of K relative to the linear conversion case shows that an optimal value exists for achieving the best resolution (see Fig. 5). K values exceeding the optimal value result in sidelobes in

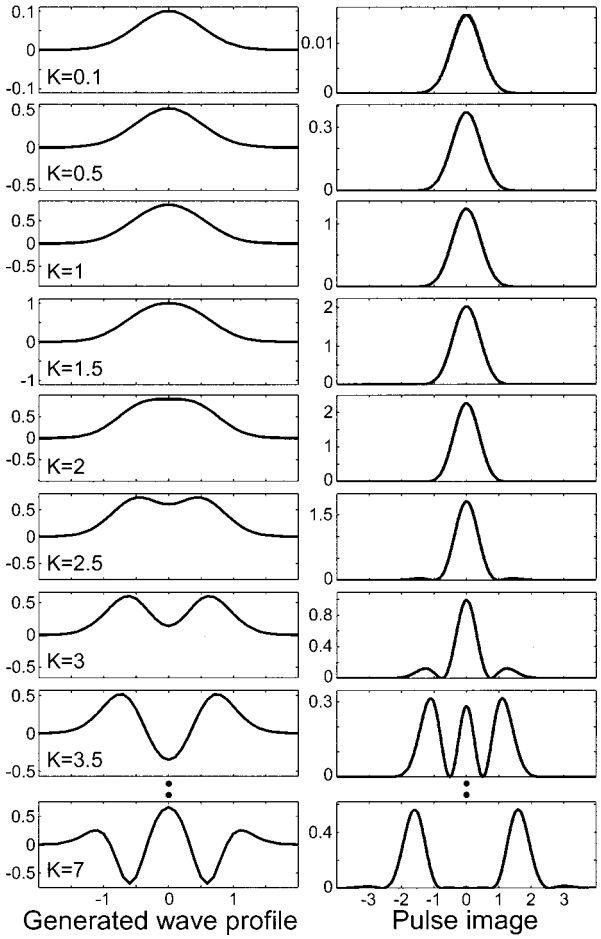

Fig. 3. Field distribution of the converted wave in the Fourier plane (left column) and the intensity distribution in the output plane after a spatial Fourier transform (right column) as a function of the reference pulse power (parameterized by K).

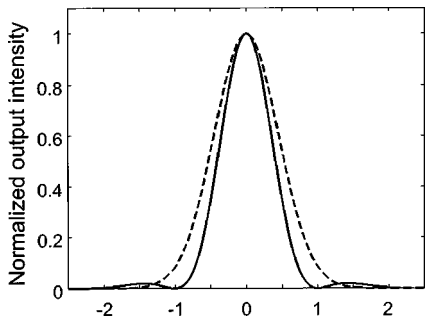

Fig. 4. Enhanced-resolution imaging: comparison of the output image for linear (dashed curve) and nonlinear (solid curve for $K = 2.5$) conversions.

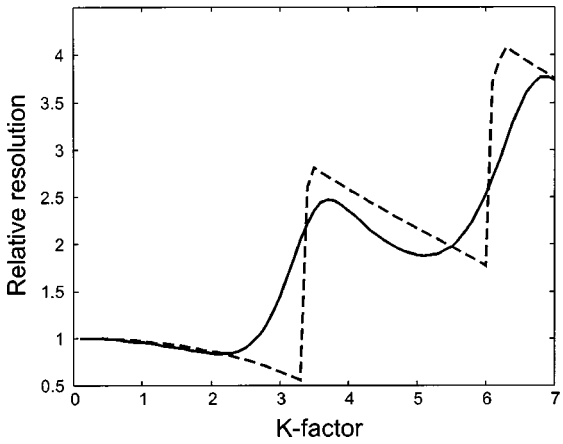

Fig. 5. Resolution improvement of the output signal as a function of reference pulse power K. Dashed curve, FWHM criteria; solid curve, standard deviation measure.

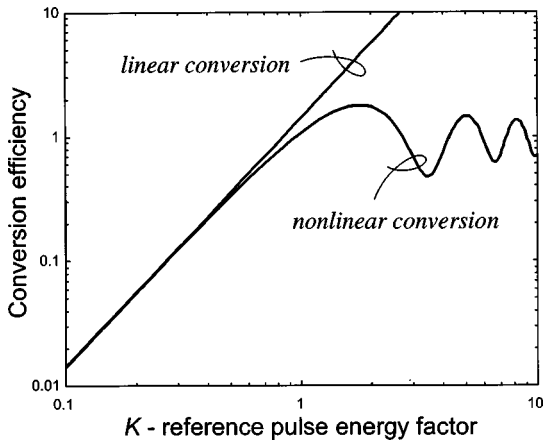

Fig. 6. Conversion efficiency as a function of reference pulse power K. The linear conversion is shown to provide acceptable results for $K < 0.5$.

the output image due to modulation in the Fourier plane, thereby reducing the resolution. The FWHM measure exhibits an abrupt increase when the intensity of the slidelobes exceeds the half-maximum value, whereas the second moment varies smoothly.

The conversion efficiency was calculated with Eq. (27) and $t_0 = 0$ as a function of K (see Fig. 6). The efficiency in the linear case [when $\sin(x) = x$ is used] is plotted as well and follows a 20-dB/dec slope. We can conclude that the linear case is applicable for $K < 0.5$. The maximum conversion efficiency is approximately 1.80, or 90% of the photons in the input signal pulse. For large values of K the conversion efficiency oscillates about 1; yet the corresponding pulse images consist of two diffracted signals and are of no interest for time-to-space conversion.

The new result predicting enhanced-resolution time-to-space mapping was observed experimentally and is described next.

5. ENHANCED-RESOLUTION EXPERIMENT

To demonstrate the enhanced-resolution time-to-space conversion, we operated the pulse imager in the nonlinear regime. We used a high-power ultrashort pulse laser producing 1-mJ pulses of 100-fs duration at an 800-nm center wavelength. The pulses were divided by a beam splitter to create a signal and a reference pulse (5% and 95% of the power, respectively). The SDW's of the pulses, generated by 600-line/mm gratings and a 375-mm lens, were mixed in a 2-mm-long β barium borate (BBO) crystal in a type I phase-matching configuration. The reference pulse power was adjusted by a neutral-density (ND) filter wheel for experimentation with different values of the parameter K. (Large ND values correspond to small values of K.) The intensity distribution of the generated wave in the Fourier plane (as opposed to the amplitude in the theoretical plots) and their corresponding output image intensity profile were detected as a function of the ND setting (see Fig. 7). As predicted in the com-

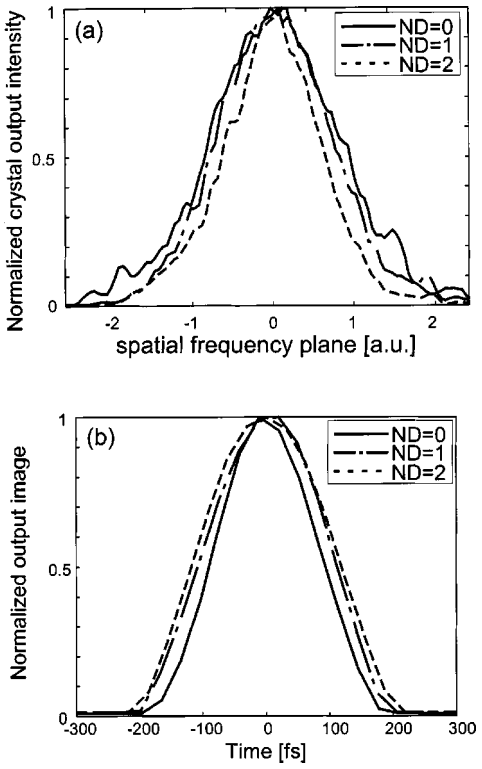

Fig. 7. Experimental results: (a) intensity distribution in the Fourier plane, (b) output pulse image, as functions of the reference pulse attenuation. A high ND setting corresponds to a small K value. Broadening in the Fourier plane and narrowing in the corresponding pulse images are exhibited.

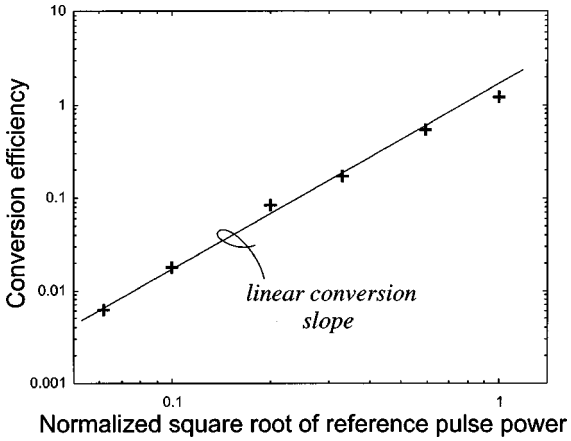

Fig. 8. Measured conversion efficiency as a function of the square root of the reference pulse power. Conversion follows the linear slope of 20 dB/dec.

puter simulation program, at a low ND setting the generated wave in the Fourier plane is broader and its corresponding output image is narrower. A plot of the conversion efficiency versus the square root of the reference pulse power shows that we are still operating in the vicinity of the linear conversion zone (see Fig. 8), as no saturation effects are observed. This can be attributed to using a Gaussian spatial mode, which varies in time, causing the nonlinear conversion to be less pronounced than in the rectangular window used in the nonlinear conversion analysis.

6. CONCLUSION

The operational characteristics of a time-to-space processor based on three wave mixing for instantaneous imaging of ultrafast waveforms has been analyzed. A model based on a Gaussian pulse envelope and a Gaussian spatial mode has been developed. This model closely describes most cases of interest, where ultrashort pulse packets from a possible optical data communication system are to be detected. Using the properties of the Gaussian model and the SPD, we define the resolution parameter of the processor. The resolution parameter dictates the observation time window for our processor and also plays a vital role in the wave-mixing process.

Both the linear and the nonlinear conversion regimes were investigated, yielding the output spatial signal form and conversion efficiency. In the linear conversion regime we find that we can define an efficiency-resolution product, which is an invariant measure depending on the system parameters. Thus efficiency can be traded for resolution and vice versa. In the nonlinear regime we show that, by using a strong reference pulse, we can enhance the spatial bandwidth of the signal, thereby achieving enhanced temporal-resolution imaging. Numerical simulation results are used to demonstrate this effect. The maximum possible power conversion efficiency was found to approach 180%. The numerical data also illustrate the operation transition point between the linear and the nonlinear regimes, which is important in the design of this processor. The nonlinear operation was also realized experimentally, demonstrating the expected enhanced-resolution performance.

The three-wave-mixing process was analyzed with the assumption of a bulk nonlinear crystal. However, it should be possible to achieve other functionalities, such as further increasing the resolution enhancement, by lateral patterning of the nonlinear crystal. This has been demonstrated in quasi-phased-matched periodically poled $LiNbO_3$, for generation of a flat-top field.[16] The same principle can be applied to the time-to-space processor, which may achieve an even finer spot size after a SFT.

APPENDIX A: PULSE AMPLITUDE AND ENERGY RELATIONSHIP

The SPD resolution was shown to depend on the input pupil size on the diffraction grating with the increasing resolution and time window at a larger pupil. For the purpose of the time-to-space converter, the nonlinear wave-mixing efficiency depends on the instantaneous input powers. When the mode on the grating is increased by use of two lenses in a telescope configuration, a larger spatial mode can be supported, but the peak power is reduced as the pulse carries finite energy. In this Appendix we find the relationship between the pulse energy and peak power by using our Gaussian pulse and Gaussian spatial mode model.

Using the expression for the input field on the diffraction grating of the SPD, Eq. (4), we find the instantaneous intensity distribution, given by

$$\begin{aligned} I_{\mathrm{in}}(x,y;t) &= \frac{1}{2}\sqrt{\frac{\epsilon_0}{\mu}}|U_{\mathrm{in}}(x,y;t)|^2 \\ &= \frac{1}{2}\sqrt{\frac{\epsilon_0}{\mu}}E_s{}^2\exp\left(-\frac{2x^2}{L_x{}^2}\right) \\ &\quad\times\exp\left(-\frac{2y^2}{L_y{}^2}\right)\exp\left[-\frac{1}{\tau^2}\left(t-t_0-\frac{\alpha x}{c}\right)^2\right]. \end{aligned} \tag{A1}$$

Using the expression for the instantaneous intensity distribution, we find the total energy on the grating, i.e.,

$$\int_{-\infty}^{\infty}\int_{-\infty}^{\infty}\int_{-\infty}^{\infty} I_{\mathrm{in}}(x,y;t)\,\mathrm{d}x\,\mathrm{d}y\,\mathrm{d}t \equiv \mathcal{E}_s,$$

and by setting the expression equal to the energy of the short pulse $\mathcal{E}_s$, we may express the field amplitude as a function of the pulse energy and pupil size, yielding

$$E_s = \left(\frac{\mathcal{E}_s}{L_x L_y \tau}\frac{4}{\pi^{3/2}}\sqrt{\frac{\mu}{\epsilon_0}}\right)^{1/2}. \tag{A2}$$

As expected, when the spatial extent increases or the pulse duration increases for fixed pulse energy, the instantaneous field amplitude decreases.

APPENDIX B: VALIDITY OF THE QUASI-STATIC APPROXIMATION FOR WAVE MIXING WITH HIGH-RESOLUTION SPECTRALLY DECOMPOSED WAVES

The effect of group velocity mismatch gives rise to temporal walk-off when we are wave mixing ultrashort pulses. Since the time-to-space processor performs the wave-mixing operation on the SDW's of the pulses, the walk-off effect is greatly reduced since the bandwidth at every point $\Delta\omega$ is smaller than the total bandwidth and the duration is extended [see Eqs. (21) and (22)]. When the Gaussian approximations for the pulse envelope and spatial mode (Section 2) are used, the bandwidths is $1/N$ of the total bandwidth.

Since in our assumptions the signal and the reference beams have the same spatial mode size L_x, they will also have the same bandwidth at any point. The phase mismatch at any location u is caused by the group velocity mismatch and is bound by $\beta\Delta\omega$ [see Eq. (24)], where β is the inverse group velocity mismatch and $\Delta\omega$ can be reduced by increasing L_x. It is possible to define a quasi-static interaction length, $L_{qs} = 1/(\beta\Delta\omega)$, which characterizes an effective length from which the effect of group velocity mismatch is perceptible. If the interaction length in the nonlinear crystal is less than the quasi-static interaction length, i.e., $L_c < L_{qs}$, then we can neglect the effect of group velocity mismatch. Thus the nonlinear wave-mixing problem can be treated in the quasi-static approximation without a partial derivative with respect to time in the differential equations characterizing the wave-propagation phenomena.

With the assumption of a high-resolution SDW, L_{qs} can be made very large, and we can use the known quasi-static solutions obtained for the case of monochromatic waves.

ACKNOWLEDGMENTS

This work was supported in part by the National Science Foundation, the Defense Advanced Research Projects Agency, and the U.S. Air Force Office of Scientific Research. Dan Marom and Dmitriy Panasenko gratefully acknowledge the support of the Fannie and John Hertz Foundation.

*Current address, Lucent Technologies, Room 4B-411, 101 Crawfords Corner Road, Holmdel, New Jersey 07733.

REFERENCES

1. P. C. Sun, Y. T. Mazurenko, and Y. Fainman, "Femtosecond pulse imaging: ultrafast optical oscilloscope," J. Opt. Soc. Am. A **14**, 1159–1170 (1997).
2. J. Janszky, G. Corradi, and R. N. Gyuzalian, "On a possibility of analysing the temporal characteristics of short light pulses," Opt. Commun. **23**, 293–298 (1977).
3. F. Salin, P. Georges, G. Roger, and A. Brun, "Single-shot measurement of a 52-fs pulse," Appl. Opt. **26**, 4528–4531 (1987).
4. A. M. Kan'an and A. M. Weiner, "Efficient time-to-space conversion of femtosecond optical pulses," J. Opt. Soc. Am. B **15**, 1242–1245 (1998).
5. P. C. Sun, Y. T. Mazurenko, and Y. Fainman, "Real-time one-dimensional coherent imaging through single-mode fibers by space–time conversion processors," Opt. Lett. **22**, 1861–1863 (1997).
6. D. M. Marom, P.-C. Sun, and Y. Fainman, "Analysis of spatial–temporal converters for all-optical communication links," Appl. Opt. **37**, 2858–2868 (1998).
7. B. Javidi and D. Painchaud, "Distortion-invariant pattern recognition with Fourier-plane nonlinear filters," Appl. Opt. **35**, 318–331 (1996).
8. R. N. Thurston, J. P. Heritage, A. M. Weiner, and W. J. Tomlinson, "Analysis of picosecond pulse shape synthesis by spectral masking in a grating pulse compressor," IEEE J. Quantum Electron. **QE-22**, 682–696 (1986).
9. A. M. Weiner, J. P. Heritage, and E. M. Kirschner, "High-resolution femtosecond pulse shaping," J. Opt. Soc. Am. B **5**, 1563–1572 (1988).
10. J. W. Goodman, *Introduction to Fourier Optics*, 2nd ed. (McGraw-Hill, New York, 1996).
11. Y. T. Mazurenko, "Holography of wave packets," Appl. Phys. B **50**, 101–114 (1990).
12. P. N. Butcher and D. Cotter, *The Elements of Nonlinear Optics* (Cambridge U. Press, New York, 1990).
13. D. Eimerl, "High average power harmonic generation," IEEE J. Quantum Electron. **QE-23**, 575–592 (1987).
14. C. Sang-Kyung, L. Ruo-Ding, K. Chonghoon, and K. Prem, "Traveling-wave optical parametric amplifier: investigation of its phase-sensitive and phase-insensitive gain response," J. Opt. Soc. Am. B **14**, 1564–1575 (1997).
15. K. Chonghoon, L. Ruo-Ding, and K. Prem, "Deamplification response of a traveling-wave phase-sensitive optical parametric amplifier," Opt. Lett. **19**, 132–134 (1994).
16. G. Imeshev, M. Proctor, and M. M. Fejer, "Lateral patterning of nonlinear frequency conversion with transversely varying quasi-phase-matching gratings," Opt. Lett. **23**, 673–675 (1998).